Measurement of exciton spin coherence by nondegenerate four-wave mixing experiments in the $\chi^{(3)}$ regime

P. Gilliot* and S. Cronenberger†
Institut de physique et chimie des matériaux de Strasbourg, GONLO, UMR 7504 ULP-CNRS, 23, rue du Læss, BP 43, F-67034 Strasbourg Cedex 2, France

H. Rahimpour Soleimani
Department of Physics, University of Guilan, P.O. Box 1914, Rasht, Iran

C. Brimont, O. Crégut, M. Gallart, and B. Hönerlage
Institut de physique et chimie des matériaux de Strasbourg, GONLO, UMR 7504 ULP-CNRS 23, rue du Læss, BP 43, F-67034 Strasbourg Cedex 2, France

(Received 28 September 2006; revised manuscript received 17 January 2007; published 26 March 2007)

We demonstrate that the spin coherence relaxation of excitons can be measured in a three-beam four-wave mixing experiment in the $\chi^{(3)}$ regime, using a sequence of contracircularly polarized pulses. In contrast to other techniques like Faraday rotation measurement, our method allows one to access spin coherence without applying an external magnetic field. The superposition of opposite spin states (exciton-polariton spin coherence) is then probed in a nondegenerate configuration at the biexciton-exciton transition. Measurements are performed on a bulk CuCl platelet. The polariton effect is taken into account by modeling the propagation of the pulses. The exciton-polariton spin coherence time is demonstrated to be mainly determined by their spin lifetime.

DOI: 10.1103/PhysRevB.75.125209 PACS number(s): 78.47.+p, 72.25.Rb

I. INTRODUCTION

In recent years, in semiconductors, nonradiative quantum coherences between electronic states that are not directly dipole coupled have attracted much attention because of their potential applications in devices and of the need to understand Coulomb correlations. In particular, spin coherence in GaAs quantum wells has been extensively studied using various nonlinear processes such as coherent Raman resonance,[1] electromagnetically induced transparency,[2] etc.

A few methods, like Faraday rotation, are used to measure the spin coherence of electronic excitations in semiconductors. They usually involve a magnetic field, which is applied perpendicularly to the propagation direction of a circularly polarized pump pulse. The spin of the photoinjected carriers precesses around this field, inducing a periodic variation of the polarization for a linearly polarized probe pulse. These quantum beats decay with the carrier spin coherence. It would be, however, interesting to remove such external perturbations and to probe only the effects of weak internal magnetic fields or pseudofields, whose fluctuations of their longitudinal component can induce a pure dephasing. Recently, a method has been proposed[3] where, in a two-beam pump-and-probe (PP) experiment, the nonlinear response of the exciton system is probed in the fifth-order $\chi^{(5)}$ regime, but where, again, a magnetic field is applied to induce quantum beats. We demonstrate here experimentally that a three beam four-wave mixing (FWM) measurement can be used to determine the spin coherence of excitons in the $\chi^{(3)}$ regime without applying any external magnetic field.

II. FWM SCHEME

A. Experimental configuration

Optical-selective excitation of well-defined electronic spin states is made possible in semiconductors by the valence band splittings: spin-orbit coupling separates the $j=3/2$ from the $j=1/2$ bands. Concerning the $j=3/2$ subbands, crystal field, stresses, or symmetry breaking effects induced by the nanoscale geometry, such as in quantum wells, can remove the degeneracy between light-hole ($j_z=\pm 1/2$) and heavy-hole ($j_z=\pm 3/2$) bands. Whatever the band is the highest, when using circularly polarized pulses, spin-polarized electron-hole pairs can be excited.[4] The momentum of the σ^+ photon is transferred to excitons in states $|+1\rangle_{lh}=|s_z^e=1/2, j_z^h=1/2\rangle$ or $|-1\rangle_{hh}=|s_z^e=-1/2, j_z^h=3/2\rangle$ [Fig. 1(a)] (the same formulas applying with opposite signs for σ^- photons to the $|-1\rangle_{lh}$ and $|+1\rangle_{hh}$ excitons). Transitions involving the split-off band, with $j=1/2$, in which we will be interested, are similar to those of the light-hole band. The exciton wave function develops thus on a large set of hole and electron

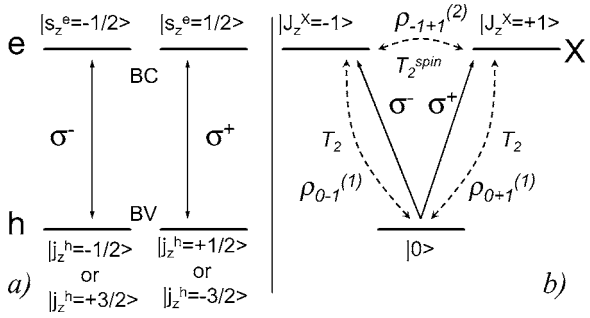

FIG. 1. (a) Four-spin-level scheme of electrons (conduction band) and holes (valence band) states described as two independent optical transitions. (b) Three-level scheme, with crystal ground state and two excitons with spin ±1, showing the optical $\rho_{0\pm1}^{(1)}$ and spin $\rho_{-1+1}^{(2)}$ coherences and the corresponding relaxation times T_2 and T_2^{spin}.

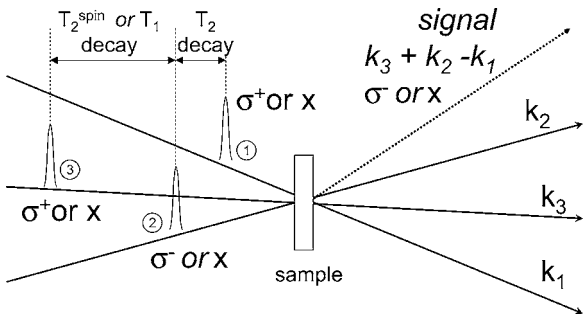

FIG. 2. Scheme of the three-pulse FWM experiment in the $\sigma^+\sigma^-\sigma^+$ and *xxx* configurations.

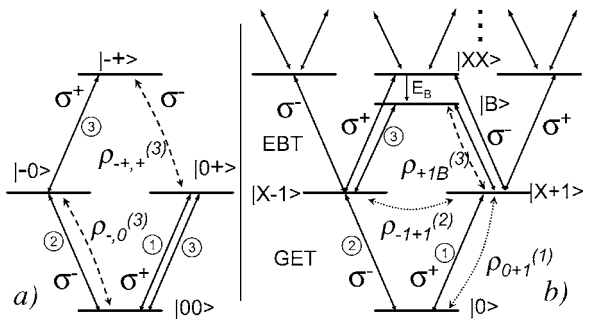

FIG. 3. (a) States of a set of two independent two-level systems. (b) Lower part of the infinite set of multiexcitonic states, with Coulomb interactions. The scheme shows the transitions involved in the FWM process (see text).

states with different wave vectors k, but with well-defined total momentum J_z^X, Fig. 1(b).

The experimental configuration of our FWM experiment takes advantages of these selection rules by using three circularly polarized beams in a contracircular polarization scheme (Fig. 2). The two first pulses are contracircularly polarized σ^+ and σ^-. They propagate along the $\mathbf{k}_1$ and $\mathbf{k}_2$ directions, respectively, and excite two different ground-to exciton-state transitions (GET's). The first σ^+ pulse induces an optical coherence $\rho_{0+1}^{(1)}$ between the ground state and the $|+1\rangle$ state (Fig. 1). It is transformed by the second σ^- pulse which excites the $|-1\rangle$ GET into a spin coherence $\rho_{-1+1}^{(2)}$ between the two excitons states $|+1\rangle$ and $|-1\rangle$. As discussed in detail below, this coherence can be probed by a third time-delayed σ^+ pulse with wave vector $\mathbf{k}_3$: it induces a nonlinear polarization $\mathbf{P}^{(3)}$ which emits a signal in the $\mathbf{k}_3+\mathbf{k}_2-\mathbf{k}_1$ direction. Measuring the signal intensity as a function of the third pulse delay allows us to determine the excitonic spin coherence decay time.

This three-beam FWM experiment scheme is similar to a configuration known for a long time as the "light-induced grating" experiment, where the two first pulses are copolarized: the first-order polarization induced by the first pulse is transformed by the second one in a second-order population grating. This population decays then with a characteristic lifetime determined by both the exciton lifetime T_1 and spatial diffusion, before being probed by the third pulse, giving also rise to a $\mathbf{P}^{(3)}$ signal in the direction $\mathbf{k}_3+\mathbf{k}_2-\mathbf{k}_1$. In the contracircular polarization configuration that we use, no populations $\rho_{+1+1}^{(2)}$ or $\rho_{-1-1}^{(2)}$ of $|+1\rangle$ or $|-1\rangle$ excitons, with a Fourier component in the $\mathbf{k}_2-\mathbf{k}_1$ direction, are created at the second-order: the only second-order term with this wave vector is a $\rho_{+1-1}^{(2)}$ coherence between the $|+1\rangle$ or $|-1\rangle$ exciton states. Nevertheless, changing the basis which is used to describe the exciton spin polarization, it can be viewed as a coherent superposition of two population gratings $\rho_{xx}^{(2)}$ and $\rho_{yy}^{(2)}$ of linearly polarized excitons $|x\rangle$ and $|y\rangle$, which are in phase opposition:

$$\rho_{xx}^{(2)} = -\rho_{yy}^{(2)} = (\rho_{+1-1}^{(2)} + \rho_{-1+1}^{(2)})/2. \quad (1)$$

In the experimental configuration we implement, a spin coherence is thus produced by a double optical excitation, taking the ground state as a bridge between the two exciton states, but without creating a population at the same $\mathbf{k}_2-\mathbf{k}_1$ point of the reciprocal space.

Both experiments, using copolarized or contrapolarized pulses and changing the delay τ_2 between the first two pulses, allow equally to probe the optical coherence of the ground–exciton-state transition and to measure its dephasing time T_2. But when the signal is measured as a function of the delay τ_3 between the second and third pulses, it is the lifetime T_1 of the excitons which is probed in the population grating experiment (which uses copolarized beams like $\sigma^+\sigma^+\sigma^+$ or *xxx*), while it is their spin coherence time T_2^{spin} which is probed in the experiment with the sequence of contrapolarized pulses $\sigma^+\sigma^-\sigma^+$ (Fig. 1).

B. Second-order coherence and third-order polarization

In the configuration we propose, the emission of a FWM signal at the third nonlinear order has to be discussed. In the scheme of Fig. 1(a), the first two pulses, which are oppositely polarized, excite two independent systems: one should expect that no coherence is induced between states which are not directly coupled and that, moreover, no nonlinear process can arise in such a configuration. We want to emphasize here two points: First, the two-$\sigma^+\sigma^-$-pulse sequence creates a spin coherence, even if one considers a set of two independent two-level systems [Fig. 1(a)]. Second, this coherence can be probed in a FWM experiment in the $\chi^{(3)}$ regime because of Coulomb interactions between excitons and biexciton formation.

Concerning the first point, we consider the whole system made of two independent two-level systems [Fig. 3(a)]. It has two single excited states $|0+\rangle$ and $|-0\rangle$ and one doubly excited state $|-+\rangle$. No connection is necessary between the two subsets to put the whole system in a coherent state $(a|-0\rangle+b|0+\rangle)$ which is the superposition of the two singly excited states. Nevertheless, this is purely formal, as this coherence cannot be probed: there is no nonlinear process that can lead to the emission of a signal in a FWM experiment. As one can show [see Fig. 3(a)], the third-order coherence $\rho_{-,0}^{(3)}$ at the transition between $|00\rangle$ ground and $|-0\rangle$ excited states interferes destructively and is canceled exactly by the contribution $\rho_{-+,+}^{(3)}$ of the transition between $|0+\rangle$ and $|-+\rangle$ states.

If one considers that a real crystal differs strongly from a two-times two-level system, one find that it can be multiexcited: Excitons, similarly to photons, are quanta of independent excitation modes of the crystal which are characterized, in particular, by their polarization—i.e., their spin. In this boson picture, too [Fig. 3(b)], there is no nonlinearity: each mode behaves like an harmonic oscillator whose response is linear and whose quanta are excitons which can be created in an infinite number.

Nonlinear processes arise when considering weak composite and interacting bosons:[5] Phase-space filling occurs because of the fermion character of the electron and hole which are bound into an exciton. The number of excitons that can be excited is thus reduced and the oscillator strength of the transitions decreases with their density. In addition, the Coulomb interaction between excitons is even more efficient to modify the crystal response, changing, for example, the energy levels of the multiexciton system as a function of the exciton spin and density. This leads to the second point that we want to stress: As shown by Palinginis and Wang,[3] coulomb interactions[6] give rise to a nonlinear polarization $\mathbf{P}^{(3)}$ and the emission of a signal through the two-exciton states. In our experiment [Fig. 3(b)], we do not use the free two-exciton states, but the bound biexciton, which ensures a connection between the two independent exciton spin states. The second-order coherence $\rho^{(2)}_{-1+1}$ is then probed at the exciton-to biexciton-state transition (EBT). This contribution $\rho^{(3)}_{+1,B}$ is no longer canceled by the signal $\rho^{(3)}_{0,-1}$ coming from the GET [Fig. 3(b)]. Moreover, it occurs at a photon energy which differs from that of the exciton transition by the binding energy of the biexciton.

C. Comparison with other experimental configurations

In our experiment, propagation directions of the incident pulses show only small angles with the normal incidence, which are further reduced by the high refraction index inside the crystal. We can thus suppose that the polarization vectors are all contained in the plane of the sample surface. Considering the polarization, the sequence of the first two contracircular pulses $\sigma^+\sigma^-$ is equivalent to a linearly polarized field whose polarization direction depends on the relative phase of the two incident pulses and is spatially modulated. It is useful to compare our experimental configuration with those of similar works. We can use the Poincaré sphere to visualize the polarization of the exciting light field: the vectors representing circular polarization $|\sigma^+\rangle$ or $|\sigma^-\rangle$ point along the z axis, respectively upwards and downwards; linear polarization vectors $|x\rangle$ and $|y\rangle$ are aligned in the equatorial plane, along the x and y axis, respectively.

The FWM scheme that we use had been suggested already by Bott *et al.*[7] Nevertheless, their description involved only a three-level scheme similar to that of Fig. 1(b) and the spin coherence was supposed to be probed at the GET transition. As discussed above, the contributions of the two-exciton levels should nevertheless cancel the signal. By measuring the signal emitted at the EBT, we take advantage here of the Coulomb interactions to avoid this destructive interference.

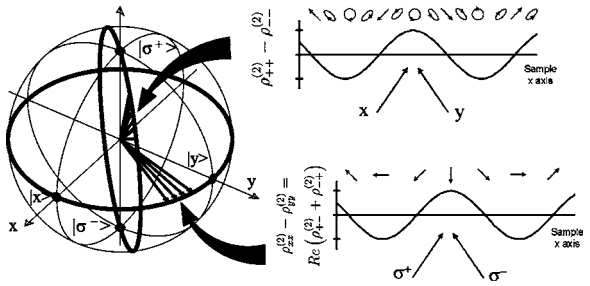

FIG. 4. Poincaré sphere. The spatial periodic modulation of the polarization orientation (lower curve), which is generated in the contracircular pulse experiment, appears as a circular trajectory of the polarization vector in the equatorial plane, while the modulation of the polarization elipticity (upper curve), which is generated in the linear cross-polarized beam experiment, is shown as a circle in a vertical plane.

A configuration very similar to ours had been also proposed by Cameron *et al.*[8] and has been used recently to study the spin relaxation of an electron gas.[9] In these three-beam FWM experiments, the two first pulses are linearly cross polarized. The polarization resulting from the sum of the two pulse fields is elliptical, with a periodic modulation in the plane of the sample surface. As a function of the spatial position, the corresponding vector on the Poincaré sphere rotates along a circle contained in a vertical plane which makes an angle of $\varphi=\pi/4$ with respect to the x axis (Fig. 4): the elliptic polarization goes periodically through the states $\pm(|x\rangle+|y\rangle)/\sqrt{2}$ and $|\sigma^{\pm}\rangle$. In comparison, in our configuration using two contracircular pulses, the resulting polarization remains always linear: on the Poincaré sphere, it rotates around the z axis (Fig. 4) on a circle which is in the equatorial plane. It goes thus periodically from $\pm|x\rangle$ to $\pm|y\rangle$ through all linear possible orientation. The contracircular pulses configuration consists thus in a spatial periodic modulation of the polarization *orientation* while the linearly cross-polarized pulses uses a modulation of the polarization *ellipticity*. In the absence of applied magnetic field, the two experiments will give the same results in an isotropic crystal, as long as exciton levels are degenerate and the linear and circular exciton basis are equivalent. Performing a spin population grating experiment in a cross-polarized linear xy configuration or performing a spin coherence experiment in a contracircular $\sigma^+\sigma^-$ configuration will thus give the same relaxation dynamics, as shown below. On the other hand, any anisotropy, like one induced by a magnetic field, can induce a difference between the longitudinal relaxation of the spin population and the transverse relaxation of the spin coherence.

In our experiment, we probe the decay of a population of linear excitons, whose orientation is spatially modulated. The same spin coherence time T_2^{spin} can be obtained in time-resolved photoluminescence (TR-PL) experiments where one measures the polarization decay of an exciton population created by linearly polarized pulses, as performed by Marie *et al.*[10] Their use of a sequence of two contracircular pulses, with a well-controlled relative phase to create the linearly polarized excitons, allows, moreover, as in our three-beam FWM measurements, to determine the optical dephasing time T_2. The differences between the two experiments are,

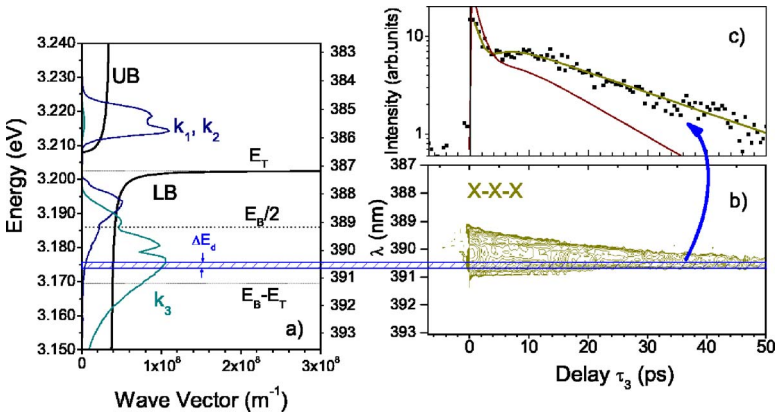

FIG. 5. (Color online) (a) Transmission spectra of the exciting pulses, showing the sample absorption. They are superimposed on the polariton dispersion curve. Exciton transition E_T and exciton-to-biexciton transition E_B-E_T energies are also displayed. (b) Intensity of the spectrally resolved FWM signal as a function of the energy detection and of the time delay τ_3 for the *xxx* configuration with colinear pulses; the delay between the first two pulses is zero $\tau_2=0$. The logarithmic plot shows 12 contour lines per decade. (c) Spectrally integrated signal in the range ΔE_d shown in part (b) of the figure. The measured points are shown together with the calculated signal (green line). In comparison, the signal for the $\sigma^+\sigma^-\sigma^+$ configuration is also displayed (red line).

first, the measurement of a second-order population in the PL experiment and of a third-order polarization in the FWM experiment; second, the way to control the phase difference between exciting pulses. It has to be temporally scanned point by point in the phase-controlled PL experiment but its modulation is spatially imprinted on the sample in one shot in our FWM experiment.

Palinginis and Wang[3] have evidenced recently the role of Coulomb interactions in the third- and fifth-order optical responses. They have shown that it is enhanced by exciton localization which consequently allows the spin coherence to be probed in the $\chi^{(3)}$ regime, while the $\chi^{(5)}$ regime is necessary for delocalized excitons. Here we show that delocalized excitons-polaritons can be probed by a third-order nonlinear process if using the biexciton transition. From an experimental point of view, Palinginis and Wang[3] perform a PP experiment involving an external magnetic field while, in our FWM measurement, we create a spin coherence which is spatially modulated in the direction $\mathbf{k}_2$-$\mathbf{k}_1$ and then we detect it in a background-free direction.

Finally, our experiment can be compared to the time-resolved Faraday measurements performed with an external magnetic field in a Voigt configuration. In such a PP experiment, the spin-polarized population of excitons which is first generated is represented by an initial vertical $|\sigma^+\rangle$ vector. It rotates around the magnetic field which is located in the equatorial plane. The temporal periodic modulation which is probed as a function of the probe pulse delay is thus similar to the spatial modulation induced in a FWM experiment by two linear cross-polarized pulses.

To create a biexciton, strict polarization selection rules are involved. If pulses are propagating almost colinearly, biexcitons can be excited only by two countercircularly polarized beams [Fig. 3(b)]. The emitted signal has thus a well-defined polarization: the coherence $\rho^{(3)}_{B+1}$ created between states B and +1 keeps the memory of the three successive pulses and of their polarization. In the $\sigma^+\sigma^-\sigma^+$ configuration, the emitted signal is thus σ^- polarized.

III. EXPERIMENTS

A. Sample description and experimental setup

We use copper chloride as a model semiconductor for our experiments. First, it has a very simple band structure. The top valence band, which is the split-off band, is only spin degenerate. Second, when compared to other semiconductors, the various contributions to the signal are here easily isolated, because of the very large binding energy (28 meV) of biexcitons in CuCl. The EBT is thus spectrally separated from the GET.[11] The sample we use in our study is a free-standing CuCl platelet, which was grown by vapor-phase transport. The crystal surfaces have [111] directions. Depending on the spot position, the thickness is found to be between 20 μm and 30 μm. For all measurements, the sample temperature is kept at 5 K in a liquid helium cryostat.

Our laser source is based on an argon-ion laser-pumped titanium-sapphire oscillator which emits 80-fs pulses at 80 MHz. The output beam is split into two parts which are separately frequency doubled in two beta baryum borate (BBO) crystals. One beam is further split into two parts to obtain two of the three pulses that excite the system. Their spectra are tuned differently by adjusting the two BBO crystals, as shown in Fig. 5(a). One of the three beams is first cross polarized with respect to the others by a half-wave plate before the polarization of all the beams is made circular by a quarter-wave plate. In order to compare our spin coherence experiment in the $\sigma^+\sigma^-\sigma^+$ configuration to measurements of the exciton population decay, we can change the polarization of the three beams to be linearly copolarized *xxx* by rotating the wave plates to their neutral axes.

The two pulses with $\mathbf{k}_1$ and $\mathbf{k}_2$ wave vectors are spectrally and temporally degenerate and are centered at the exciton resonance [Fig. 5(a)]. They are polarized with opposite helicities σ^+ for $\mathbf{k}_1$ and σ^- for $\mathbf{k}_2$. They induce a spatial modulation of the exciton spin orientation with a wave vector $\mathbf{k}_2-\mathbf{k}_1$. These two pulses are short, approximately 150 fs, and cover totally the exciton resonance but not the EBT. The

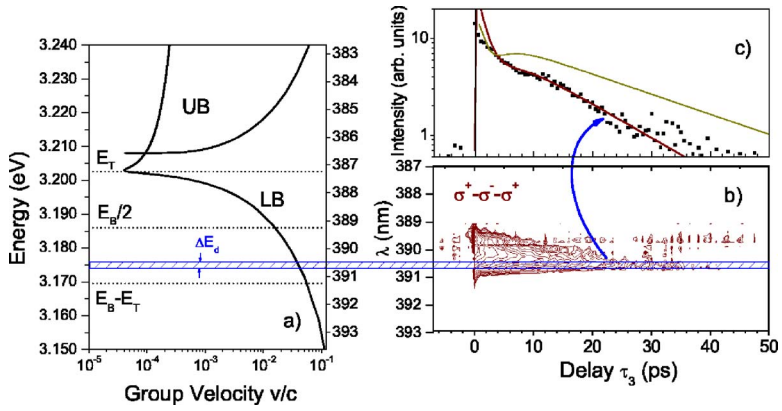

FIG. 6. (Color online) (a) Group velocity of the polaritons as a function of their energy, calculated from the dispersion curve of Fig. 5(a). Exciton transition E_T and exciton-to-biexciton transition E_B-E_T energies are also displayed. (b) Intensity of the spectrally resolved four-wave mixing as a function of the energy detection and the time delay τ_3 for the FWM configuration $\sigma^+\sigma^-\sigma^+$ used to measure the exciton spin coherence decay; the delay between the first two pulses is zero $\tau_2=0$. The logarithmic plot shows 12 contour lines per decade. (c) Spectrally integrated signal in the range ΔE_d shown in part (b) of the figure. The measured points are shown together with the calculated signal (red line). In comparison, the signal for the *xxx* configuration is also displayed (green line).

third $\mathbf{k}_3$ pulse is centered at lower photon energy, close to the EBT, and is σ^+ polarized. It induces a signal at the $|B\rangle$ to $|X,+1\rangle$ EBT, in the direction $\mathbf{k}_3+\mathbf{k}_2-\mathbf{k}_1$, which is σ^- polarized. The intensity of the emitted signal is measured as a function of the delay τ_3 between the third pulse and the two first ones.

B. Experimental results

The data obtained in the $\sigma^+\sigma^-\sigma^+$ configuration are shown in Figs. 6(b) and 6(c) in comparison with the data obtained in the *xxx* configuration, shown in Figs. 5(b) and 5(c). When $\tau_3>0$ the $\mathbf{k}_3$ pulse arrives on the sample after the $\mathbf{k}_1$ and $\mathbf{k}_2$ pulses. In both configurations, the diffracted signal shows oscillations in the first 10 ps which are followed by an exponential decay. But we observe that the dynamics in the $\sigma^+\sigma^-\sigma^+$ configuration is different from that of the *xxx* configuration.

To analyze the data, one has to consider three types of third-order nonlinear processes (Fig. 7) that occur in PP as well as FWM experiments within the ground-state–exciton–biexciton system. The Pauli blocking (PB) is due to the population of the excitonic levels and is described by population $\rho_{\pm1\pm1}$ or coherence $\rho_{\mp1\pm1}$ second-order terms of the density matrix between exciton states $|X\pm1\rangle$. It gives rise to a signal at the GET. The same density matrix terms are involved in a signal generation at the EBT which is seen as an induced absorption (IA) in a PP measurement. Last, the second-order coherence ρ_{0B} due to the two-photon transition (TPT) from the ground state $|0\rangle$ up to the biexciton $|B\rangle$ give rise to a signal at both the GET and EBT. The efficiency of these processes will depend on the pulse temporal order. It will be also strongly determined by the photon energy of the pulses and the spectral position of the detection, because the direct excitation of biexciton states implies that the sum of the energies of the two involved photons or excitons must be equal to the biexciton energy. This explains the spectral shape of signals plotted in Figs. 5(c) and 6(c).

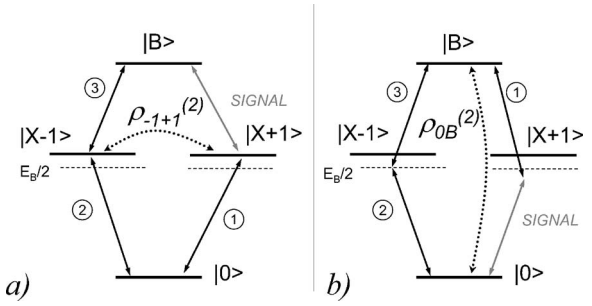

FIG. 7. Nonlinear processes involved in the FWM signal: (a) induced absorption (IA) and (b) two-photon transition to the biexciton (TPT).

Close to E_B-E_T, which is the difference between the biexciton energy E_B and the transverse exciton energy E_T, the signals are mainly due to the IA process. An exciton population, in the case of a *xxx* configuration (Fig. 5), or an exciton coherence, in the case of a $\sigma^+\sigma^-\sigma^+$ configuration (Fig. 6), is created by the $\mathbf{k}_2$ and $\mathbf{k}_1$ pulses at the GET and a signal is emitted at the EBT with the energy E_B-E_T. Nevertheless, exactly at this position, the spectral components of both the third $\mathbf{k}_3$ exciting pulse and the emitted signal are strongly reabsorbed in the sample thickness, biexcitons being created from the exciton population.

For larger photon energies, close to the half of the biexciton energy $E_B/2$, the FWM signals are dominated by the TPT process. For the signal emitted in the $\mathbf{k}_3+\mathbf{k}_2-\mathbf{k}_1$ direction, a coherence is induced by the $\mathbf{k}_2$ and $\mathbf{k}_3$ pulses between the ground and the biexciton states. The $\mathbf{k}_1$ pulse induces then the emission of the signal.

The spectral and temporal shape of the signal is also strongly modified by the polariton effect which is especially strong in CuCl. The resulting dispersion curve is plotted in Fig. 5(a). It gives rise to large effects on the pulse propagation, because of the large variation of the group velocity with energy, as shown in Fig. 6(a). Indeed, the spectral components of the three exciting $\mathbf{k}_{1,2,3}$ pulses which are involved in the different FWM processes travel with different velocities.

The order and the delays of the exciting pulses can thus be strongly modified with respect to their incident values. This has mainly consequences on the TPT part of the signal. To create the second-order coherence between ground and biexciton states, the $\mathbf{k}_3$ pulse has to catch up with the $\mathbf{k}_2$ pulse within the sample thickness. This must be done before the arrival of the $\mathbf{k}_1$ pulse, which will induce the signal emission.

This explains the faster decay, when approaching $E_B/2$, of the TPT contribution to the signal. As discussed above, it is the most important in this spectral region [Fig. 6(b)], where the IA signal is very weak. The sum of the spectral components of the $\mathbf{k}_1$ pulse and of the signal being equal to the biexciton energy, they are symmetrically located on both sides of $E_B/2$. An increase of the detection spectral position implies a decrease in the corresponding $\mathbf{k}_1$ pulse spectral component energy having a higher group velocity [see Fig. 6(a)]. This results in a signal which is stopped more and more quickly, as a function of the delay τ_3, when approaching $E_B/2$: When changing the detection photon energy from 3.175 eV down to 3.186 eV ($E_B/2$), the corresponding spectral component of the $\mathbf{k}_1$ pulse which is involved in the signal emission, varies from 3.197 eV to 3.186 eV. Its group velocity increases then from $2\times10^{-3}c$ up to $2\times10^{-2}c$ and the time to travel the 20-μm sample thickness at these speeds decreases from 30 ps down to 3 ps [Fig. 6(b)].

We are nevertheless mainly interested in the IA absorption contribution to the FWM signal in the $\sigma^+\sigma^-\sigma^+$ configuration. The coherence created by the $\mathbf{k}_1$ and $\mathbf{k}_2$ between opposite spin excitons will be probed by the third pulse. Same considerations apply to the exciton population measurements in the *xxx* configuration. The spectral region E_d we choose is shown by two lines in Figs. 5(b) and 6(b). As discussed below, it is close to the EBT energy E_B-E_T to maximize the IA contribution to the signal and to minimize the TPT contribution.

C. Data modeling

All the points discussed above have been carefully verified by modeling the systems and performing numerical simulations of the FWM experiments. This allows us also to verify that within the spectral range we choose, the signal is determined by the IA process.

In order to take into account the effects of polariton propagation, we have solved numerically Maxwell-Bloch equations in which the propagation of the electromagnetic field is given by the Maxwell equation and the response of the system is given by the optical Bloch equations. We use the level scheme of Fig. 7 and consider all three nonlinear processes (PB, IA, and TPT). The electric field is split into three parts: $E(z,t)=E_1(z,t)+E_2(z,t)+E_3(z,t)$, where $E_i(z,t)$ represents the pulse propagating in the direction $\mathbf{k}_i$. It is easy to obtain the expression of the third-order polarization $P^{(3)}$ propagating in the direction $\mathbf{k}_3+\mathbf{k}_2-\mathbf{k}_1$. The procedure to include the propagation effects is given in details in Refs. 12 and 13, but no further approximations are made here. In the calculation we assume a linear pulse propagation. The linear response of the four-level system would thus lead to the well-known polariton dispersion relation in the same way as a two-level system. The pulses are assumed to be colinearly propagating in the crystal in the z direction. The model is not restricted to the special configuration that we study here and has been probed for a large set of configurations, changing the pulse order, their photon energy, and their polarization.

The simulation reproduces well the intensity of the FWM signal as a function of energy detection E_d and time delay τ_3 in the range $E_d \in [3.186\ \text{eV}, 3.174\ \text{eV}]$—i.e., roughly between the $E_B/2$ and the E_T-E_B energies. As discussed above, for energies close to 3.186 eV, the signal is dominated by a two-photon absorption process and we cannot obtain information about the decay of the grating (population lifetime or spin coherence time, depending on the excitation conditions). For energies close to $E_B-E_T=3.1695$ eV, the EBT energy, the experiment is not reproduced by the simulation because at these energies the spectral components of pulse 3 are strongly absorbed and a nonlinear propagation occurs. In the spectral region we choose, nonlinear propagation is not of relevance and the FWM dynamics is driven by the IA process between exciton and biexciton states. Our simulation confirms that, as explained above, this is achieved in the spectral region E_d, shown in Figs. 5(b) and 6(b), in which we integrate the signal.

The result of the integration is displayed in Figs. 5(c) and 6(c) for both experimental data and modeling. We observe that, in the first 10 ps, the dynamics is relatively complicated. This is due to interference effects between the TPT and IA terms. However, for longer time delays, the decay becomes monoexponential. In the case of the *xxx* configuration [Fig. 5(c)], the simulation well reproduces the dynamics of the experimental signal for the following parameters: $d=30$ μm, $T_2=6$ ps, and $\tau_x=42$ ps. τ_x is the decay time of the FWM signal, which includes both the exciton lifetime T_1 and the decay of population grating due to the ambipolar diffusion of the carrier $\Gamma_G=4\pi^2D/\Lambda$, where D is the ambipolar diffusion coefficient and Λ the grating wavelength. T_2 can be measured by varying the delay between pulses 1 and 2. This had been performed[14] under similar conditions, and a value of 1.7 ps had been found. The slight discrepancy may be due to the fact that T_2 depends strongly on the photon energy, the excitation density, and the sample. From induced absorption experiments,[11] we know the exciton lifetime to be $T_1=80$ ps and we can thus determine $1/\Gamma_G=88$ ps. We estimate d from the dynamics driven by the two-photon term which gives a precise value of the sample thickness, even if this parameter has no significant influence in the region E_d. In Fig. 6(d) is shown the result for the $\sigma^+\sigma^-\sigma^+$ configuration. The value of $\tau_\sigma=30$ ps is found to be the best value of the decay to fit the experimental curve. Taking into account the carrier diffusion contribution Γ_G, we obtain the value of the spin coherence time $T_2^{spin}=45$ ps. The spin lifetime has also been measured in previous experiments[11] and is $T_1^{spin}=60$ ps.[19]

D. Exciton-polariton spin decay in CuCl

From the experiments described above we thus obtain the following values for the excitonic dynamics: The exciton lifetime is $T_1=80$ ps (this can be compared to the value of

70 ps obtained by induced absorption measurements[15]) and the optical coherence of the excitonic transition (GET) is $T_2=6$ ps. The spin lifetime is $T_1^{spin}=60$ ps while the spin coherence time is $T_2^{spin}=45$ ps. A part of the spin coherence decay is due to the population losses of the two states $|X,+1\rangle$ and $|X,-1\rangle$, while the other contribution would be pure dephasing $T_2^{spin^*}$:

$$\frac{1}{T_2^{spin}}=\frac{1}{T_1}+\frac{1}{2T_1^{spin}}+\frac{1}{T_2^{spin^*}}. \tag{2}$$

Removing the contribution of the excitonic recombination $1/T_1$, we obtain the transverse spin relaxation time

$$\frac{1}{T_\perp^{spin}}=\frac{1}{2T_1^{spin}}+\frac{1}{T_2^{spin^*}} \tag{3}$$

while the longitudinal spin relaxation time is given by

$$\frac{1}{T_\parallel^{spin}}=\frac{1}{T_1^{spin}}. \tag{4}$$

From our data, we see that $T_\perp^{spin}=103$ ps and $T_\parallel^{spin}=60$ ps. In an isotropic material, the transverse and longitudinal spin relaxation times should be equal. Nervetheless, in a cubic zinc-blende crystal with T_d point-group symmetry like CuCl, the electron-hole exchange interaction has very important consequences for the exciton spin relaxation: First, it lifts the degeneracy between the dipole inactive exciton state (having a total angular momentum $J=0$) and the dipole active states (corresponding to $J=1$). In CuCl the splitting energy $\Delta_{st}=2.5$ meV.[16] In addition, due to the strong exciton photon coupling (polariton effect), it also leads to a splitting between the longitudinal ($J=1$, $J_z^x=0$) and the two transverse exciton states ($J=1$, $J_z^x=\pm 1$). The splitting energy is $\Delta_{LT}=5.5$ meV (Ref. 16) in CuCl. The degeneracy of the two transverse excitons can be further lifted due to the symmetry breaking of the wave vector **Q**, which couples the two transverse exciton states. The coupling strength depends on the absolute value of the wave vector and on the direction of propagation (it goes to zero in the [111] direction[16,17]). If one develops the interaction Hamiltonian into powers of **Q**, one finds that matrix elements of the coupling between the states[17] are small ($<8\times10^{-3}$ meV) in the polariton bottleneck region. Therefore, one can neglect the longitudinal and the triplet exciton states and consider only the nearly degenerate transverse states. In the two states subspace of transverse excitons ($J=1$, $J_z^x=\pm 1$), the symmetry breaking of the wave vector **Q** can be looked at as an effective magnetic field. Up to second order in **Q**, the diagonal elements of the interaction are always equal but the nondiagonal elements can be different from zero. This corresponds to a pure transverse effective magnetic field which couples the states. Fluctuations of the wave vector lead to spin relaxation, which can have different origins: Fluctuations of the longitudinal magnetic field lead to fluctuations of the energy splitting between the two circularly polarized states. This affects the Rabi frequency and gives rise to pure dephasing. But since the longitudinal effective magnetic field component is always zero and does not fluctuate, it leads to zero pure dephasing $1/T_2^{spin^*}=0$. In this approximation, from Eq. (3), we deduce that $T_\perp^{spin}=2T_\parallel^{spin}$ as observed in our experiments. If one includes cubic terms in **Q**, one finds that they do not depend on the electron-hole exchange interaction but involve only single electron or hole spin flips. They are at the origin of the D'yakonov-Perel interaction.[18] This interaction is diagonal in the basis of the two transverse exciton states, lifts their degeneracy, and gives rise to a purely longitudinal effective magnetic field. As explained above, its fluctuation would lead to a pure dephasing $1/T_2^{spin^*}\neq 0$, but we consider it to be negligible, since the absolute value of the wave vectors is too small in the polariton bottleneck region.

IV. CONCLUSION

We have shown that, using a three-beam FWM configuration with contracircularly polarized pulses, the spin coherence of excitons can be directly determined in the $\chi^{(3)}$ regime. The coherence induced by the two first pulses is probed by the third one at the EBT, in a nondegenerate experiment. The data analysis needs to take into account polarization effects and their propagation, as well as the various nonlinear processes which generate a signal in the exciton-biexciton system. We observe a spin transverse relaxation time of 103 ps, which is nearly twice the longitudinal one around 60 ps, showing that no pure dephasing of the exciton spin occurs. This is explained by the symmetry breaking induced by the exciton propagation and the transverse polarization of dipole-active excitons.

*Pierre.Gilliot@ipcms.u-strasbg.fr

†Present address: Groupe d'étude des semiconducteurs, GES, UMR 5650 CNRS, Université Montpellier 2, place Eugène Bataillon, F-34095 Montpellier Cedex, France.

[1] M. Lindberg and R. Binder, Phys. Rev. Lett. **75**, 1403 (1995).

[2] M. Phillips and H. Wang, Phys. Rev. Lett. **89**, 186401 (2002).

[3] P. Palinginis and H. Wang, Phys. Rev. Lett. **92**, 037402 (2004).

[4] G. Lampel, Phys. Rev. Lett. **20**, 491 (1968).

[5] T. Ostatnický, P. Gilliot, and B. Hönerlage, J. Lumin. (to be published).

[6] K. B. Ferrio and D. G. Steel, Phys. Rev. Lett. **80**, 786 (1998).

[7] K. Bott *et al.*, J. Opt. Soc. Am. B **13**, 1026 (1996).

[8] A. R. Cameron, P. Riblet, and A. Miller, Phys. Rev. Lett. **76**, 4793 (1996).

[9] S. G. Carter, Z. Chen, S. T. Cundiff, A. S. Huntington, and L. A. Coldren, in *Conference on Lasers and Electro-Optics/Quantum Electronics and Laser Science Conference and Photonic Applications Systems Technologies 2006 Technical Digest* (Optical Society of America, Washington, D.C., 2006), QME6.

[10] X. Marie, P. Le Jeune, T. Amand, M. Brousseau, J. Barrau, M.

Paillard, and R. Planel, Phys. Rev. Lett. **79**, 3222 (1997).
[11] H. Rahimpour-Soleimani, S. Cronenberger, O. Crégut, J.-P. Likforman, M. Gallart, T. Ostatnický, P. Gilliot, and B. Hönerlage, Appl. Phys. Lett. **85**, 5263 (2004).
[12] T. Takagahara, Phys. Rev. B **31**, 8171 (1985).
[13] P. Schillak and I. Balslev, Phys. Rev. B **48**, 9426 (1993).
[14] E. Vanagas, J. Kudrna, D. Brinkmann, P. Gilliot, and B. Hönerlage, Phys. Rev. B **63**, 153201 (2001).
[15] R. Leonelli, A. Manar, J. B. Grun, and B. Hönerlage, Phys. Rev. B **45**, 4141 (1992).
[16] B. Hönerlage, R. Lévy, J.-B. Grun, C. Klingshirn, and K. Bohnert, Phys. Rep. **124**, 161 (1985).
[17] H. Rahimpour-Soleimani, T. Ostatnický, S. Cronenberger, M. Gallart, P. Gilliot, and B. Hönerlage, J. Appl. Phys. **100**, 023705 (2006).
[18] M. I. D'yakonov and V. I. Perel, Sov. Phys. JETP **33**, 1053 (1971).
[19] In Ref. 11, we found a time constant $\tau_s = 120$ ps, for the decay rate of a $|X, \pm 1\rangle$, exciton spin. We define here T_1^{spin}, as the decay constant of the exciton spin population difference, with $T_1^{spin} = \tau_s/2 = 60$ ps.